PERGAMON

Journal of Structural Geology 22 (2000) 1247–1260

JOURNAL OF STRUCTURAL GEOLOGY

www.elsevier.nl/locate/jstrugeo

Fault controlled sequential vein dilation: competition between slip and precipitation rates in the Austin Chalk, Texas

Young-Joon Lee[a,b], David V. Wiltschko[b,*]

[a]*Korea Institute of Geology, Mining and Materials, Taejon 305-350, South Korea*
[b]*Department of Geology and Geophysics, Center for Tectonophysics, Texas A&M University, College Station, TX 77843-3115, USA*

Received 6 July 1998; accepted 5 April 2000

Abstract

Multi-layered calcite veins in a dilatant jog of a left-stepping, left-slipping shallowly buried fault segment are composed of alternating millimeter- to submillimeter-thick calcite veinlets and host lithons forming a coarse 'crack–seal' texture. The grain fabrics in calcite veinlets are mostly equant or irregular, suggesting face-controlled grain growth in a fluid-filled cavity. The relatively thick veinlets can be developed by progressive fault slip and veinlet opening simultaneously with calcite precipitation under low effective stress. Continuous changes in the oxygen isotopic compositions of the calcite veinlets along the length of veins suggest that the individual calcite veinlets were sequentially developed from the footwall to the hanging wall. There is no particular evidence that these veins represent excursions in fluid pressure or instantaneous fracture opening related to episodic fault slip; the fracture formation and filling cycle could have taken place along a continuously slipping fault contained within a porous rock with normal fluid pressure.

1. Introduction

Veins record the fluid composition, precipitation conditions and perhaps the kinematics of vein wall motion during vein mineral precipitation. The internal structures may include: (1) equant to fibrous mineral habits; (2) micrometer-scale to centimeter or decimeter veinlets or mineral sheets; and (3) micrometer to centimeter or decimeter single inclusions or curviplanar sheets, to name common varieties. In some veins displaying a fibrous mineral habit, the fabrics of the vein minerals record syntaxial or antitaxial growth (Durney and Ramsay, 1973). Recent work with fibrous veins displaying the 'crack–seal' texture (Ramsay, 1980) indicates that mineral fiber axes may not be reliable indicators of opening direction (Urai et al., 1991). However, in many veins the net opening direction is decipherable by matching opposing vein walls.

In this paper we describe a multi-layered or compound vein composed of alternating veinlets and host material caught between two shear surfaces. Because of the size of the veinlets and intervening host lithons, it is possible to resolve optically and subsequently reconstruct the opening kinematics of this vein with some confidence. Veins of this sort have been described by others from other tectonic regimes (e.g. Gaviglio, 1986; Labaume et al., 1991; Davison, 1995). Veins of this type are significant because: (1) they are restricted to dilatant jogs of en échelon, probably overlapping, fault segments; (2) the effective confining pressure appears to be low; and (3) they have been previously interpreted as representing episodic vein opening by the 'crack–seal' mechanism (Davison, 1995). The last interpretation we will alter somewhat.

The particular sample described here is a hand specimen-scale multi-layered calcite shear vein displaying alternating tabular host lithons and veinlets (terminology from Lee et al., 1997). Its opening sequence was first recognized by a change in oxygen isotopic values along the vein length (Lee et al., 1997). In this paper

* Corresponding author. Fax: +1-409-845-3002.
E-mail address: d.wiltschko@tamu.edu (D.V. Wiltschko).

0191-8141/00/$ - see front matter
PII: S0191-8141(00)00045-6

we characterize the vein kinematics related to the fault slip events.

2. Geological setting of the vein

The calcite vein examined is from the upper Cretaceous Austin Chalk Formation exposed in the Longhorn Cement Company quarry near San Antonio, Texas. This quarry is located in an Austin Chalk outcrop belt which extends from Dallas in the north to Del Rio in southwest Texas (Fig. 1). Although the timing of deformation is not well constrained, all structures can be associated with normal fault systems related to the extension of the Gulf of Mexico (Jackson, 1982; Brown et al., 1983; Collins et al., 1990). The depth of burial was between 1 and 2.7 km, probably more nearly the former (Grabowski, 1984; see discussion in Lee et al., 1997).

Calcite veins are exposed in vertical walls within of the Longhorn Quarry. The chalk here consists of nearly flat-lying massive chalk beds of 1–1.5 m thick separated by thin shaley limestone beds. The chalk mainly consists of very fine-grained carbonate mud with coarse skeletal grains. The average calcite content is 88%. The grain size of the chalk matrix ranges from 0.5 to 4.0 μm and the porosity ranges from 6 to 30% (Cloud, 1975).

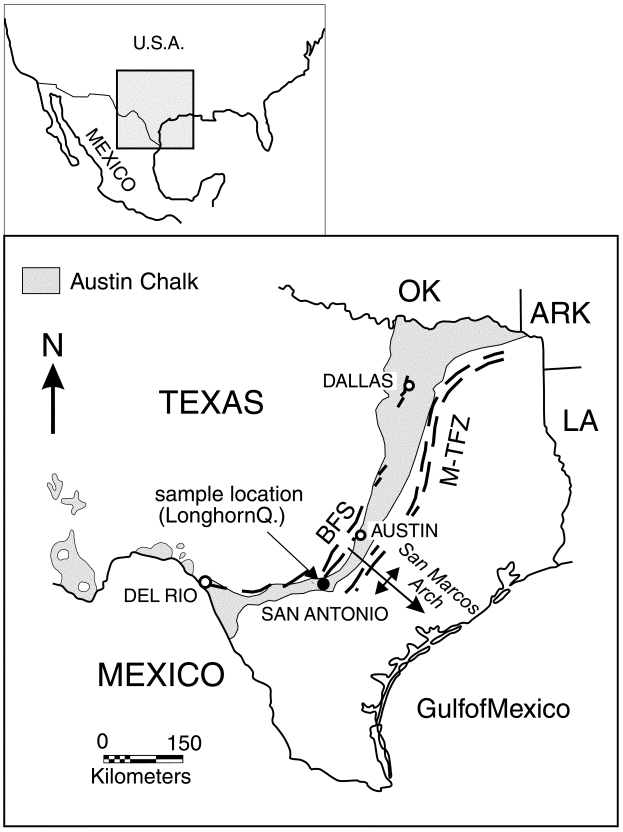

Fig. 1. Map of Austin Chalk outcrop trend (shaded). Vein samples are from the Longhorn Quarry at San Antonio, Texas. BFS: Balcones fault system, M-TFZ: Mexia-Talco fault zone (modified after Corbett et al., 1987).

Fig. 2(a) shows a calcite vein emplaced along a 40° NW dipping synthetic fault associated with a high angle normal fault; bedding dips a few degrees to the NW. The vein sampled is in a left-stepping, left-slipping en échelon dilational jog in the fault. The normal fault segments overlap in the region of vein formation.

3. Vein structures

3.1. Terminology

The vein described in this study is representative of others we have examined throughout the outcrop belt of the Austin Chalk. It is composed of alternating tabular calcite veinlets and host lithons. The veinlets have been variably called calcite fill or veins by Labaume et al. (1991), but we prefer the former term because it differentiates the secondary material in the vein (millimeter scale) from the overall structure (centimeter–meter scale). We define the vein structure as multilayered to emphasize the internal structure but these same features have been described earlier as 'tabular calcite' (Labaume et al., 1991) or 'compound' (Gaviglio, 1986) veins. Labaume et al. (1991) used the term matrix bands or septa for what we call host lithons. Ramsay (1980) originally described such wall-rock slivers in crack–seal textures as 'wall-rock inclusion bands'.

3.2. Observations

Within the vein, calcite grains in the veinlets are mostly equant (Fig. 2c). The grain size increases away from the veinlet wall, sometimes with an indistinct suture line along the center (arrow in Fig. 2c; see also Gaviglio, 1986). Grain size also seems to be roughly proportional to the thickness of the veinlet in that thicker veinlets contain larger grains. Unlike the veins described by Labaume et al. (1991), the calcite grains do not show any evidence of crystal-plastic deformation such as mechanical twinning or crystallographic or grain-shape preferred orientation; evidently the veinlets never experienced a differential effective stress sufficient to cause mechanical twins in calcite (approximately 20 MPa; Heard in Friedman, 1967).

The host lithons do not exhibit observable differences in either grain size or texture from the surrounding massive chalk at hand specimen, thin section, or SEM scales. The individual host lithons are typically less than a millimeter in thickness. The shape of the host lithons varies from simple thin quasi-parallel

sided layers (less than 0.3 mm thick) to large rhombic sections (star in Fig. 3b near isotope site H5). Both calcite veinlets and host lithons are truncated along a surface parallel to the main vein wall (central truncation surface: CTS for brevity in Fig. 3b; see also Fig. 2c). In this and other samples, these truncation surfaces are not always continuous through the vein but are always parallel to the main slip surfaces. In the third dimension, this and all other veins in this outcrop are essentially identical to those described by Labaume et al. (1991) (their fig. 7) and also Jessell et al. (1994) (their fig. 8).

Both veinlets and host lithons generally make an angle of 62° (standard deviation 19°) with the vein walls, which are also fault slip surfaces (Fig. 3). The opening direction of the veinlets is near parallel to the main slip surface. The thickness of calcite veinlets varies from 0.1 to 2 mm, measured normal to the veinlet wall. The width of a veinlet measured parallel to the main slip surface is fairly constant at any position along the veinlet length, even though some of the veinlets curve and consequently change thickness, measured normal to the veinlet walls, along their lengths. Measured parallel to the CTS, the veinlets are on average thicker than the host lithons (mean 0.5 mm vs. 0.3 mm; Fig. 4a, b). Veinlets are typically thicker than adjacent host lithons (Fig. 4c). Opposite veinlet walls match.

The opening sequence of the vein was established by stable isotope analyses of both calcite veinlets and host lithons. There is a large oxygen isotopic change from veinlet to veinlet along the vein. The calcite veinlet $\delta^{18}O$ values linearly decrease from −2.6 to −5.6‰ (PDB) and to −5.4‰ (PDB) along lines X and Y, re-

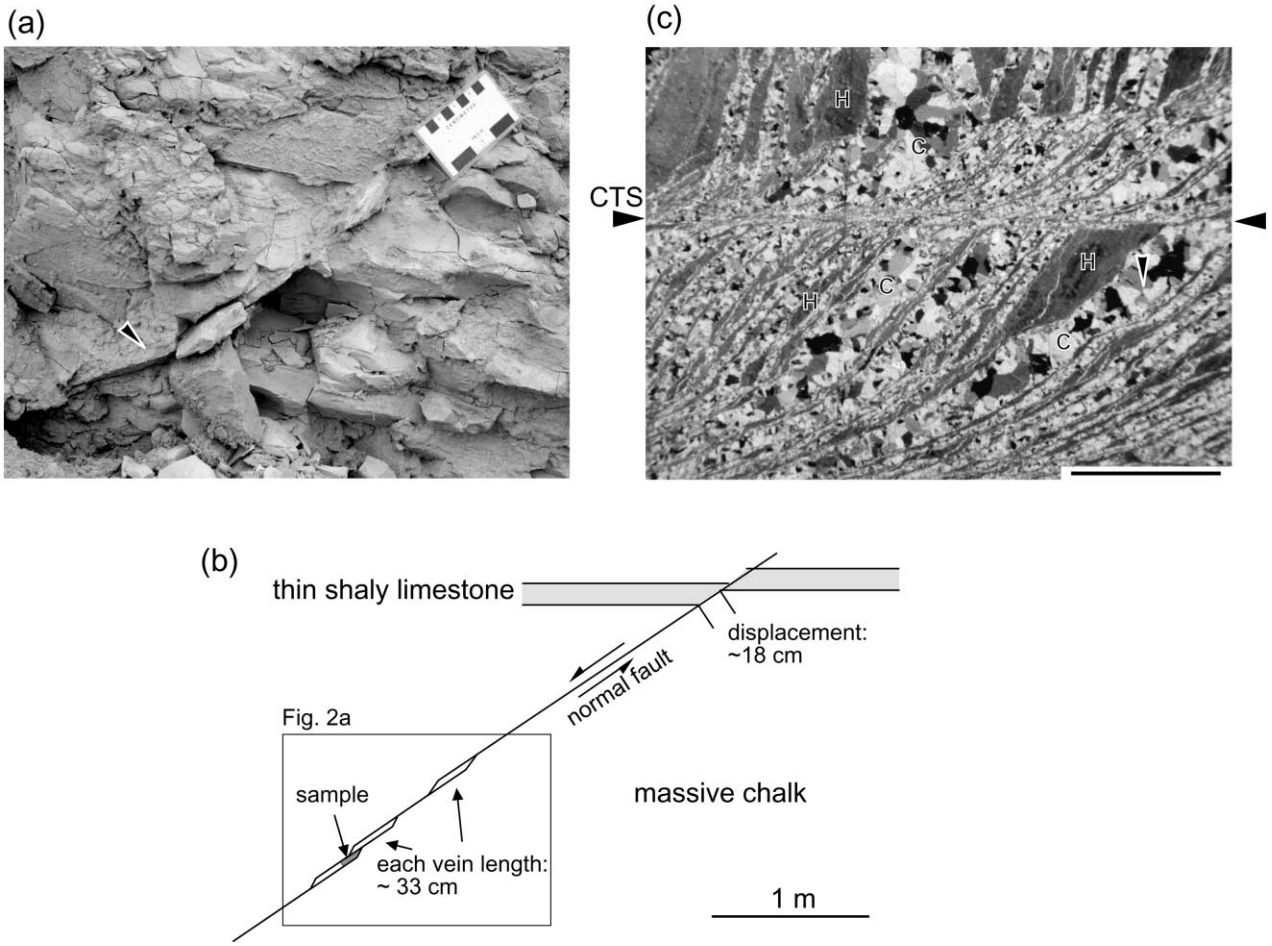

Fig. 2. (a) Multi-layered calcite vein along a NW-dipping fault indicating the exact location of the sample (arrow) analyzed in this study. The length of the scale card is 9 cm. (b) Schematic diagram showing the relationship between the displacement of the fault containing the vein in (a) and the vein length in the vertical outcrop. The apparent displacement of the fault as measured by the shear vein length is about 33 cm. This value is much larger than fault slip measured from bedding offset (about 18 cm) along the same fault due to the inclusion of host rock in the vein. (c) Photomicrograph of the vein texture showing alternation of calcite veinlets (C) and host lithons (H). The calcite veinlets are composed of mechanically untwinned, equant calcite grains, sometimes showing indistinct median sutures lines (arrow). A central truncation surface (CTS), indicated by arrows at the both sides of the photo, is developed parallel to the fault slip planes. The scale bar is 3 mm. The position of the photo is located in Fig. 3(b). Cross-polarized light.

spectively (Fig. 3b). On the other hand, $\delta^{18}O$ values for the host lithons vary only slightly from −2.9 to −3.8‰, except H3. The $\delta^{13}C$ values of both calcite veinlets and host lithons lie in a relatively narrow range from +1.2 to +1.9‰, except one analysis (H1) (+2.5‰).

An interpretation of the isotopic data related to the opening and precipitation history of the vein is provided by Lee et al. (1997). The veinlet calcite became progressively depleted in $\delta^{18}O$ probably due to the successive addition of deeper, hotter fluids during vein precipitation (Lee et al., 1997). This interpretation is supported by: (1) the estimated ratio of fluid to vein calcite volume ratio; (2) trace elements; and (3) fluid inclusion results. Textural evidence also indicates the direction of CTS propagation. For the sample in Fig. 3, the veinlet opening started from the footwall side and progressed toward the hanging wall side. Other veins in the same outcrop show similar structural and geochemical characteristics (see Lee et al., 1997).

3.3. Characteristics of the veinlet and host lithon in each domain

The vein may be divided into domains based on

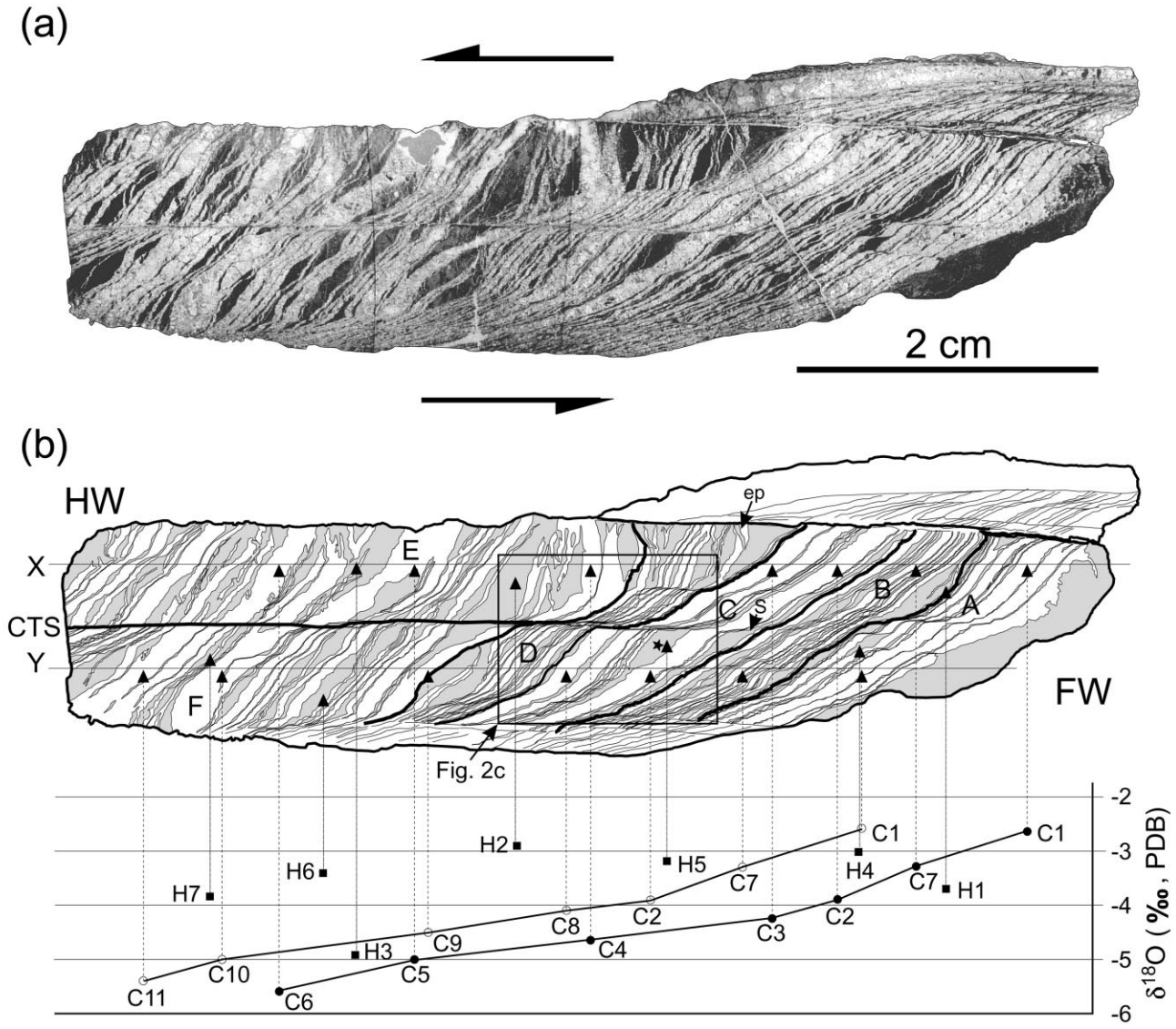

Fig. 3. (a) Photomicrograph of the vein sample. Dark layers represent host lithons and light ones are calcite veinlets. Plane-polarized light. (b) A traced diagram of (a) describing individual components of the vein. The vein was divided into six domains mainly based on structural discontinuities such as truncation surfaces and changes in opening width and frequency. Tracing was not possible for some parts along the bottom and for a small tapered part located above a truncation surface in the upper right corner. CTS: central truncation surface; S: start of the CTS; star symbol: abnormally thick, rhombic host lithon; ep: en passant fracture. The oxygen isotopic compositions for calcite veinlets along lines X and Y decrease linearly from footwall (FW) towards hanging wall (HW). Positions for isotope analyses are labeled.

changes in veinlet thickness from footwall to hanging wall. In Domain A, the veinlets are asymptotic toward the bottom of the vein. In addition, small, sharp jogs in fracture orientation develop parallel to the major slip direction. Even so, individual veinlets are continuous. The average calcite veinlet thickness is more than three times larger than that of the host lithons. The thickness of both calcite veinlets and host lithons is relatively constant through the domain.

The thickness of the calcite veinlets in Domain B is half that of Domain A. Veinlet walls are relatively straight. The veinlets and host lithons are equal in thickness across this domain.

The veinlet thickness increases again in Domain C. The central truncation surface starts to develop in this domain. On the right side of the domain, there is a 1.5 mm apparent displacement between the upper and lower parts of a calcite veinlet. An abnormally thick, non-parallel sided host lithon that occurs just below the truncation surface also marks this boundary (star near isotope site H5 in Fig. 3b). The orientation of the veinlet walls in the upper part is near parallel to that in Domain B, but in the lower part, the orientation becomes steeper in going down through the truncation surface. The veinlet misalignment between the upper and lower parts along the truncation surface increases to about 3 mm with the introduction of another host lithon of variable thickness.

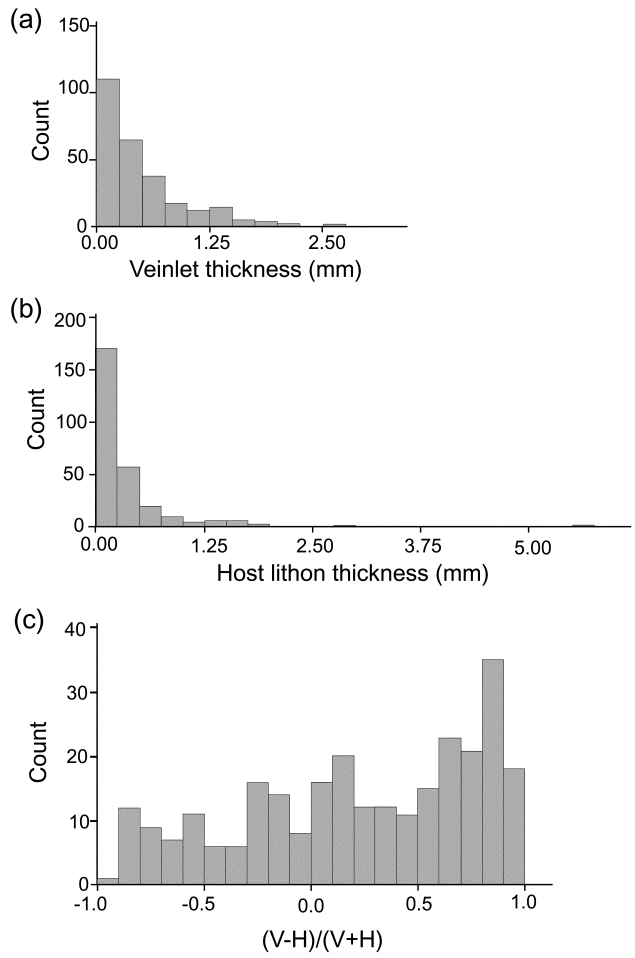

Fig. 4. Histograms showing the distribution of the thickness of both veinlets and host lithons. (a) Veinlet. Mean = 0.5 mm. (b) Host lithon. Mean = 0.3 mm. (c) Relative thickness of a veinlet to an adjacent host lithon. (V–H): veinlet–host lithon. (V + H): veinlet + host lithon. A value of −1.0 on the abscissa represents zero vein thickness whereas + 1.0 represents zero host thickness.

Domain D shows a somewhat different texture from other domains. The thickness of the calcite veinlets is less than that in Domain C, yet similar to that in Domain B. The large central truncation surface continues with a constant misalignment. It is still possible to trace the individual veinlets and host lithons across the surface. Another local truncation surface develops in the upper part of Domain C (see Figs. 2c and 3). The inclination of the veinlets to the vein wall is approximately 70° in the upper part of the domain, changing to 40° at the truncation surface. Above the local truncation surface, calcite veinlets sometimes terminate within a host lithon in going from the wall of the vein inward. Host lithons in this part are relatively thick and irregularly shaped. There is a suggestion of en passant fracture tip interaction in the upper right corner of this quadrant (ep, in Fig. 3b). Individual calcite veinlets and host lithons are not continuous across the boundary in Domains E and F, although the veinlets in the two domains developed simultaneously. The estimated misalignment between the two domains is about 3 mm as determined by both oxygen isotopes (Fig. 3b) and structural similarities such as frequency and opening amount of veinlets. The misalignment amount along the truncation surface does not change from Domain C. In Domains E and F, the thickness of both the calcite veinlets and the host lithons is not constant and their alternating patterns are irregular. Two 1.3-mm-thick veinlets intervened by a thin host lithon and one 2.0 mm veinlet occur in that area. In summary, veinlet thickness appears cyclic from Domain A to D. Domains of large veinlets (Domains A and C) alternate with domains of small veinlets (Domains B and D).

4. Kinematic analysis of the vein

4.1. Restoration of vein displacements

This vein shows a protracted textural history, which makes it possible to assess its kinematics. The individual host lithons from the deformed-state diagram in Fig. 3(b) were moved together by removing the calcite veinlets based on: (1) the veinlet wall geometry; (2) opening amount; and (3) direction starting from the hanging wall (Domains E and F) (Fig. 5). It was im-

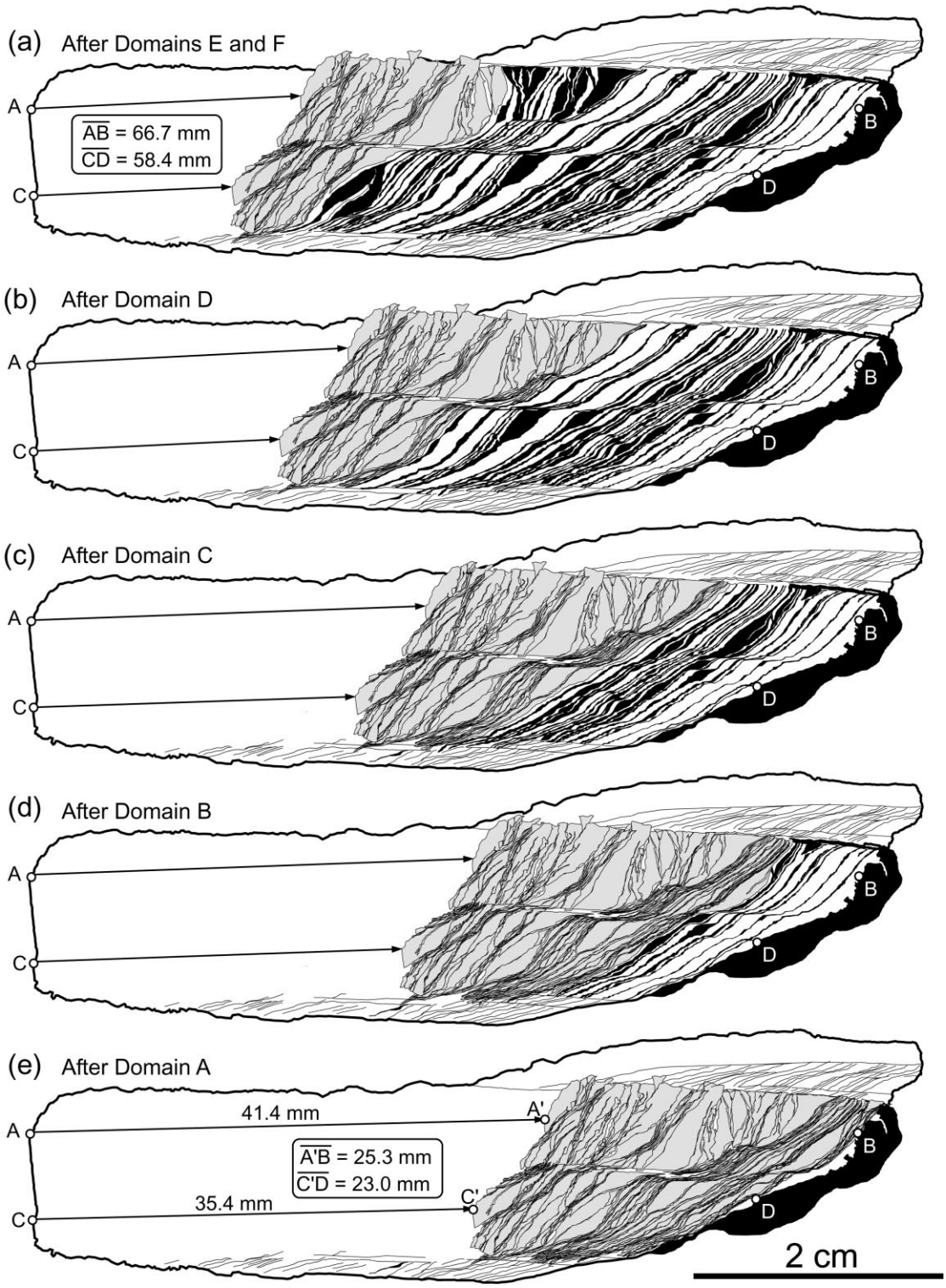

Fig. 5. Sequential restoration of the vein from (a) to (e). The vein formed from (e) to (a). Black layers: host lithon. White layers: calcite veinlet. Gray parts indicate the restored host lithons to the undeformed state. The white area of the vein in the upper right was not restored, but is shown for reference. Labels for each part, e.g. 'After Domains E and F' refer to the stage in the restoration after the named domains are collapsed.

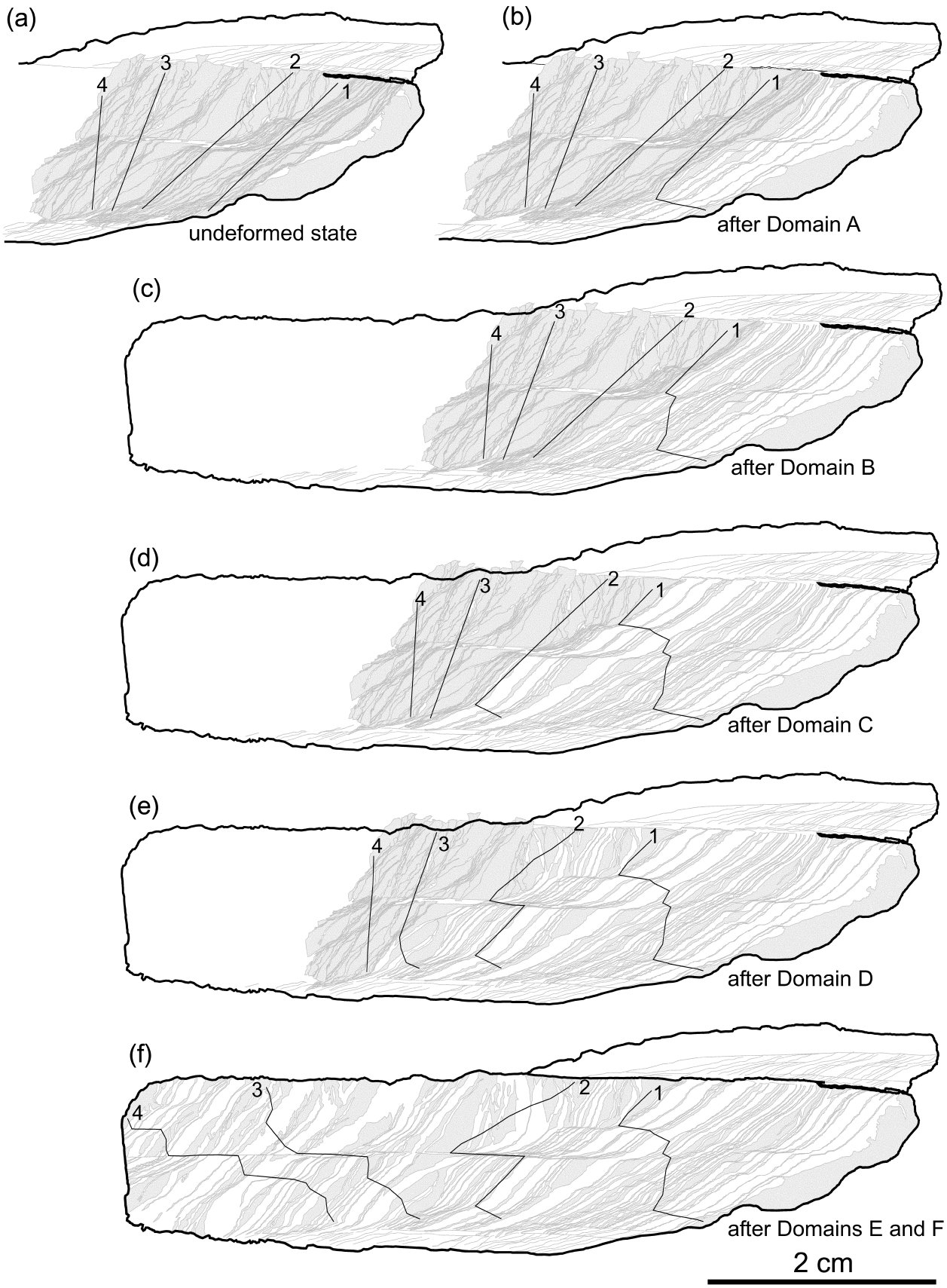

Fig. 6. Evolution history of four initially straight lines with vein development. See text for an explanation.

possible to reconstruct the opening in the portion of Domain A next to the footwall because of the ambiguous boundary of the large host piece at the right end of the vein. Some boundaries do not fit well resulting in small gaps or overlaps. However, the degree of such boundary mismatching is small relative to the size of the vein. Some relatively large gaps exist along the central truncation surface (CTS in Fig. 3b). It appears that the host lithons near the central truncation surface might have become ground down or disaggregated during slipping between Domains E and F. As the central truncation surface is not straight, a small clockwise rotation (~3°) is required to restore the left half of the vein.

The deformed-state (Fig. 3b) lengths A–B and C–D in Fig. 5(a) are 66.7 and 58.4 mm, respectively. The undeformed lengths are 25.3 and 23.0 mm for A′–B and C′–D, respectively. Therefore, the opening amounts represented by this vein along A–B and C–D are 41.4 and 35.4 mm, respectively (Fig. 5e). Because the sample is only a part of a longer vein (see Fig. 2a), the ratio of true opening to apparent opening for the vein sample was calculated to estimate the true displacement of the fault reflected in the whole vein. The ratios along those two lines A–B and C–D are 0.62 (41.4/66.7) and 0.61 (23.0/58.4), respectively. Based on these data, we can estimate that about 60% of the vein sample length corresponds to opening and deposition of veinlet material whereas the remaining 40% consists of the intervening host lithons. In outcrop (Fig. 2b), the total measured apparent vein length is about 33 cm but the fault offset on a shale-rich layer is only about 18 cm (i.e. 55% of the vein length). Therefore, the vein dilation calculated from the reconstruction closely represents the fault offset.

4.2. Progressive deformation in the vein

This vein shows a complicated texture over a distance of only 7 cm. Four initially straight lines, assumed to be fixed with respect to host lithons, were drawn on the undeformed-state diagram (Fig. 6a) and tracked as each domain formed (Fig. 6b–f). It was assumed that a line across the two walls of a veinlet remains continuous throughout the deformation. The evolution history of the four lines illustrates the cyclic opening behavior from Domain A to D. It also clarifies the amount and true sense of slip across the central truncation surface between Domains E and F.

The final morphology of Line 1 shows a W-shape (Fig. 6e). This indicates that the strain was inhomogeneous and periodic in space due to alternation of small and large openings of veinlets. There is a 2 mm counterclockwise misalignment of line 2 along the central truncation surface (Fig. 6e). The misalignment of line 2 increases to about 5 mm in Domains E and F. Lines 3 and 4 are similarly misaligned in a left-lateral sense, indicating that net opening was relatively constant from Domain C onward (Fig. 6f). The fact that lines 3 and 4 are roughly straight as compared to lines 1 and 2 suggest that the alternation of large and small veinlets shown from Domain A to D ceases in Domains E and F. Instead, irregular-sized veinlets develop on both sides of the central truncation surface later in this vein's history (Fig. 7).

5. Discussion

5.1. Mechanisms of vein formation

The vein discussed here formed between two left-slipping, left-stepping segments of a small displacement normal fault. The initiation and growth of the vein as well as some of the internal features may be explained with reference to the local stress field that existed at the time of vein formation. (1) The region between two left-stepping, left-slipping normal faults will experience reduced mean stress (Segal and Pollard, 1980; Ohlmacher and Aydin, 1997). If the background effective mean stress is low, the minimum principal stress may be tensile (Fig. 8). (2) Segal and Pollard (1980) found that there is a region of reduced tensile stress between the two fault segments which might reduce the tendency for fractures to continue from one fault segment tip to the other (Segal and Pollard, 1980, fig. 11b). (3) The trajectories of the Mode I cracks become asymptotic to the body of the fault segment opposing a fault tip (see Fig. 8b). Ohlmacher and Aydin (1997) show that the orientations of the secondary or bridging fractures are a function of both the friction on the fault segments and the orientation of the remote applied stress.

Although direct application of models such as these to natural examples is problematic, several of the observations are consistent with predictions of the above models. (1) The veinlets appear to originate as Mode I cracks; (2) the CTS may reflect the inability of some of these cracks to propagate through a region of reduced tensile stress and thus link both fault segments; and (3) the veinlets become asymptotic to the footwall fault segments; (4) the angle between the fault and veinlets (about 60°) in light of the presumed orientation of the remote stress suggests that the friction of the fault was low. Alternatively, the range of possible values for the remote stress is 30–70° to the fault (Ohlmacher and Aydin, 1997); low-angle shear to the fault seems unlikely. These results match the observations that the calcite in the veinlets contains no mechanical e-twin lamellae, suggesting a differential stress less than 20 MPa.

Fig. 9 shows the hypothetical development of a

multi-layered vein. As slip takes place, the inclined curved fracture, initiated as a Model I crack, opens parallel to the slip direction and calcite-supersaturated fluid migrates into the open space. Equant calcite precipitates because the opening is large enough for face-controlled grain growth. The successive Mode I cracks occur preferentially in the host rock near the preceding calcite veinlet rather than either at the boundary with a calcite veinlet or inside the calcite veinlet (Fig. 9b). Hulin (1929), Labaume et al. (1991) and Davison (1995) suggest that this occurs because host rock is weaker than vein material. We would add that if precipitation takes place not only in the vein proper but also within the nearby pore space of the host, the strength of that part of the otherwise porous rock will increase. This cementation may move the boundary between strong vein material and weaker matrix into the matrix itself. Cracking would, therefore, preferentially develop in less cemented parts of the host chalk. However, it is not clear that the observed variable thickness of host lithons is entirely controlled by this process.

Central truncation surface may be initiated due to heterogeneities in the host rock (Labaume et al., 1991) and then propagate as secondary shear planes within host rock (Gaviglio, 1986) (Fig. 9c). Although we have not observed fossil fragments or other inhomogeneities spawning truncation surfaces, the lack of complete knowledge of the third dimension makes it impossible to say that they do not exist. Perhaps the kinks in crack path leading to a truncation are caused by fractures twisting around the object or as a result of a local change in shear direction, causing twist hackles or crack breakdown in the third dimension. A local increase in effective mean stress may be a contributing factor. Truncation surfaces are an end-on view of these breakdown segments, which are subsequently linked. Labaume et al. (1991) assert that the truncation surfaces grow in the direction in which they are attenuated. We reach the opposite conclusion based on the following mechanism for the fracture opening model related to the development of shear planes in a given stress system as well as the reconstruction of this vein based on the opening direction implied by the isotope data.

Fig. 10(a) shows an isolated shear fracture in a sinistral shear regime. At one tip of the fracture the local stress state is either compressive or tensile above or

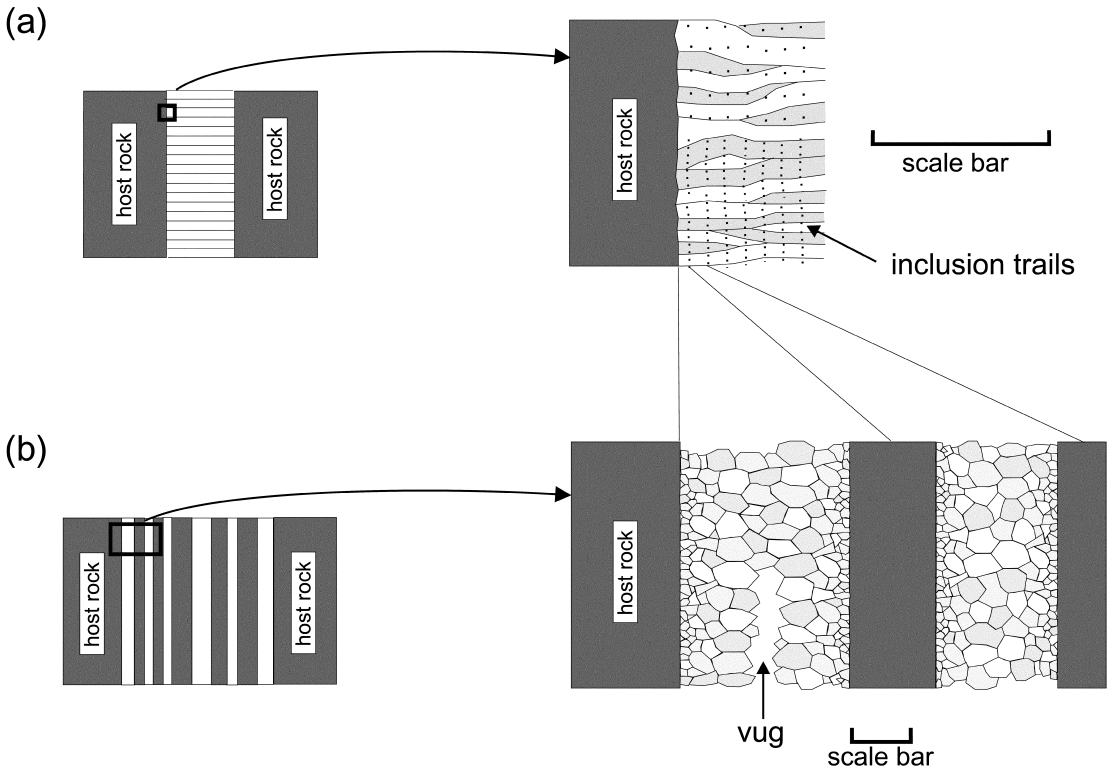

Fig. 7. Comparison between the geometries of (a) fibrous 'crack–seal' vein and (b) multi-layered vein. No similarity in mechanism for the formation of the two geometries is necessarily implied. Note that if all but every fourth or fifth inclusion is eliminated along a host-parallel inclusion plane, then the inclusion trails remaining appear to be normal to the host wall. These host-normal trails have been described by Jessell et al. (1994). A distinguishing characteristic between these two types of vein filling patterns is the suppression of competitive grain growth in veins termed 'crack–seal.' In the multi-layered vein veinlets, competitive grain growth leads to both larger grains in the middle of veinlets and larger medial grains in thicker veinlets.

below, respectively, the fracture. At the other fracture tip the compressive and tensile fields are reversed. The trajectories of σ_1 are inclined at a low or high angle to the shear plane, for compressive or tensile, respectively, and asymptotic to the remote stress (Ohlmacher and Aydin, 1997). As the veinlet openings are initiated as Mode I cracks they may represent the local σ_1 trajectories at the time of opening. Therefore, the shapes of veinlets at the two tips are different (Fig. 10b, c). Consequently, this asymptotic veinlet geometry can be an indicator for the direction of CTS propagation. In Domains C and D of the vein sample (see Fig. 3), the overall veinlet shapes are similar to that in Fig. 10(b). This fact indicates that the CTS propagated from the footwall side toward the hanging wall side accompanying sequential veinlet opening. This textural evidence, also exhibited in other vein samples (see Lee et al., 1997), supports the conclusion from oxygen isotope data that this vein developed from the footwall toward the hanging wall.

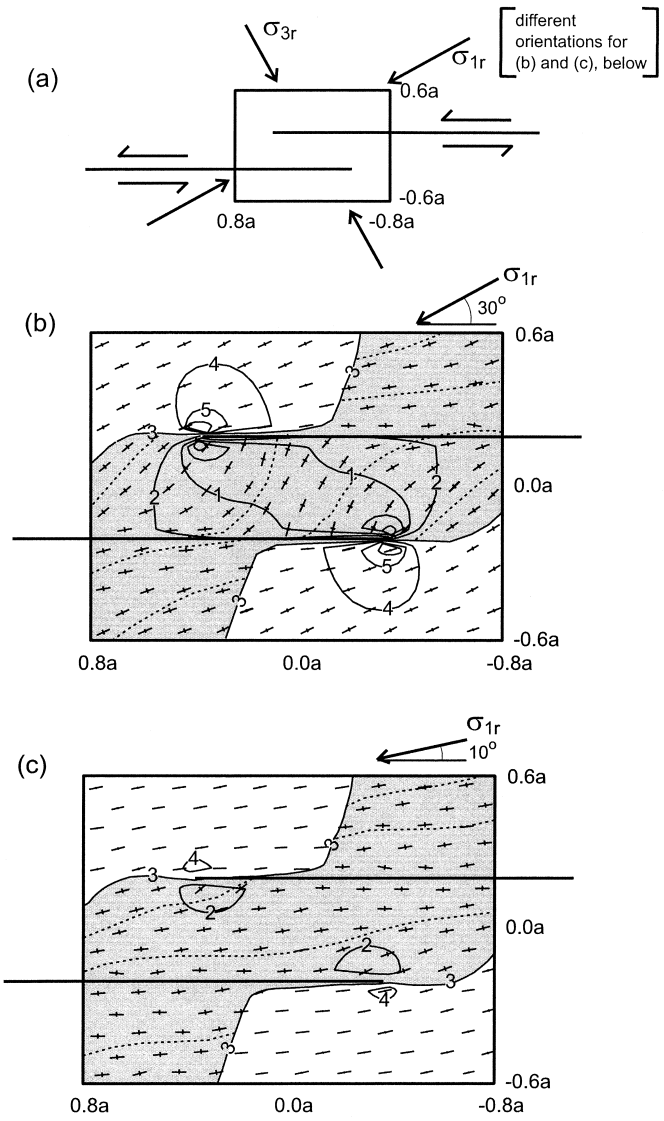

Fig. 8. Plots of the orientation of σ_1, potential new cracks, and the magnitude of the mean stress between two left-stepping, left-slipping fault segments, after Ohlmacher and Aydin (1997). The coefficient of friction on the faults is 0.0001. (a) Key diagram showing remote principal stresses (σ_{1r}: greatest compressive) and region covered by (b) and (c) relative to the faults included in the models. a is the half length of each of both faults and dimension unit of (b) and (c). (b) σ_{1r} 30° to the faults. (c) σ_{1r} 10° to the faults. Crosses in both (b) and (c) indicate local stress trajectories, the long bars the maximum principals stress trajectories and the short bars the minimum. Shaded areas are those where tensile failure is favored due to reduced mean stress. Contours (thin lines) are in mean stress where 1.0 is the applied remote minimum principal stress. Potential new Mode I fracture surfaces are plotted as dashed lines within the shaded portion of each plot. The maximum mean stress is higher for (b) than (c). The potential new Mode I crack orientations in (b) have a similar shape to the veinlets observed in both our sample and those of others. Shallow veinlets consistently make a small angle with the bounding faults.

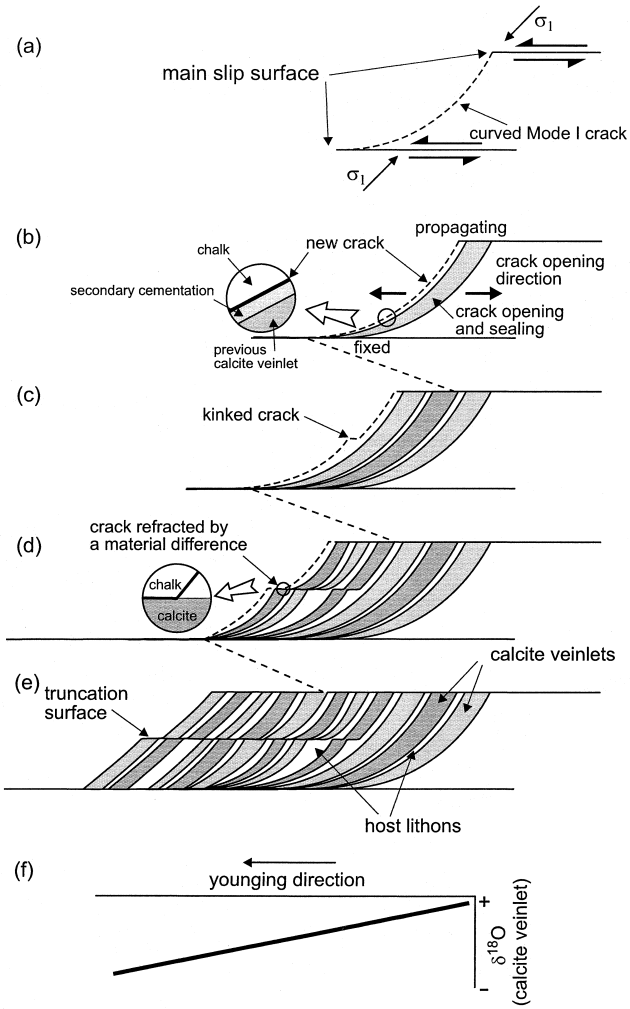

Fig. 9. (a)–(e) Schematic diagrams showing the evolution of a simulated multi-layered crack–seal vein with the development of alternating calcite veinlets (shaded) and host lithons. (f) Oxygen isotopic values of the calcite veinlets decreasing linearly with the vein evolution. See text for discussion.

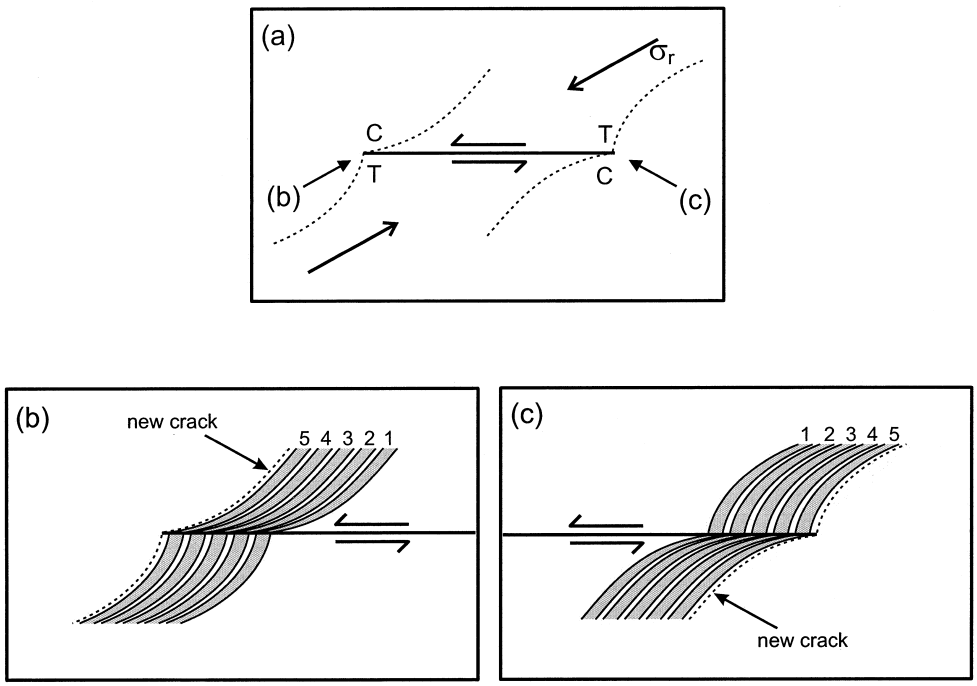

Fig. 10. (a) Schematic diagram showing the local σ_1 trajectories at the tips of an isolated shear fracture in a sinistral shear regime. σ_r: remote maximum compressive stress. C: compressive region. T: tensile region. (b) and (c) Differences in the geometry and sequence (1 = oldest) of curved veinlet openings at each end of a propagating shear fracture.

Along the truncation surface, the apparent sense of the veinlet misalignment is opposite to the sense of slip on the bounding fault. The true slip sense of the vein can be determined by reconstructing the relative displacement of host lithons along the truncation surface (see Fig. 6f). The truncation surface continues to develop with further crack openings, the geometry of subsequent cracks follows that of the existing veinlets. In some cases, the orientation of subsequent cracks may be influenced by a difference in materials that exist across the central truncation surface (Fig. 9d). This may also result in the kinked crack openings. The repetitive dilational process produces a large multi-layered vein with the observed isotopic profile (Fig. 9e, f).

5.2. Relationship between opening and filling processes in multi-layered veins

Whether sequential veinlet formation reflects continuous or episodic fault slip is not known (compare Gaviglio, 1986; Davison, 1995). In Fig. 11 we show the possible relationships between the opening and the precipitation for episodic and continuous slip scenarios. If the fault slips episodically, the opening of an initial crack would accompany a fault slip event. Precipitation would occur in the suddenly produced open space and proceed to completion because the crack provides a pathway for mass flux to the crack walls. A new veinlet forms during some later slip event in the adjacent weaker portion of the host (Fig. 11a). If instead the fault slips continuously (Fig. 11b), we envision stable crack propagation from the en-échelon fault segments as illustrated in Figs. 9 and 10. Assuming that delivery of calcite to the crack is not the rate limiting process, calcite precipitation, initially slow on small grains, quickens on larger crystals with better-oriented growth surfaces (see Fig. 2c). Alternatively, precipitation may speed up due to the propagation of the crack in three dimensions, enhancing connectivity,

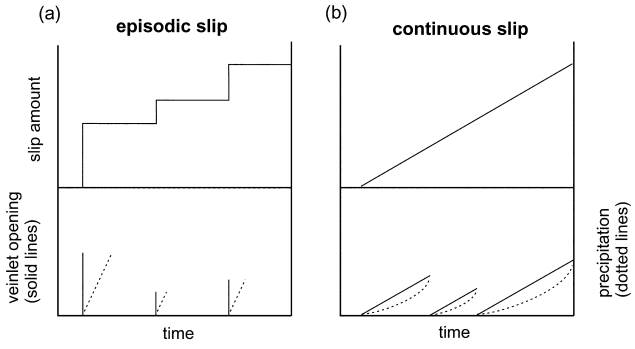

Fig. 11. Schematic diagrams showing the relationship among veinlet opening, fault slip, and precipitation with time. It is not necessary for individual opening episodes to occur within the same time interval. In (a), the openings occur instantaneously, whereas in (b), individual openings progressively develop with vein precipitation. The precipitation rate was assumed to be constant through the entire vein filling process.

and thereby increasing the mass flux to the veinlet. If the rate of fracture dilation is slower than the rate of calcite precipitation, filling will eventually overtake opening and the veinlet will completely fill. The timing of complete filling of the veinlet is a function of a trade off between dilation rate and precipitation rate. Once completely sealed, the veinlet is strong relative to surrounding host, and a new fracture will propagate stably into unveined host. Therefore, the fault slip rate could have been constant but variations in precipitation and dilation rate explains the repetitive opening (Fig. 12)

5.3. Comments on veins generally termed crack–seal

For discussion purposes, it is useful to compare the texture, mechanism for vein filling and deformation mode of the multi-layered veins and veins termed crack–seal (e.g. Durney and Ramsay, 1973; Ramsay, 1980; Etheridge et al., 1984; Cox, 1987; Fisher and Brantley, 1992; Jessell et al., 1994) (Fig. 7). The two major points of comparison are distances between inclusion sheets or host lithons and grain fabrics. The multi-layered calcite vein in this study is composed of relatively wide veinlets, typically 0.3–1 mm thick filled with mostly equant calcite grains; intervening host lithons are similar in thickness to that of the veinlets. In veins termed crack–seal individual vein segments between inclusion sheets are typically 5–100 μm thick (e.g. Ramsay, 1980; Ramsay and Huber, 1987, p. 576; Fisher et al., 1995). The vein filling is typically fibrous, although not in all cases (Cox and Etheridge, 1983, p. 166 et seq.; Cox, 1987). Unlike the multi-layered vein described here, inclusions in veins termed crack–seal may also be new crystals precipitated from the same solution as the predominant vein mineral (i.e. mica inclusions in quartz veins); the inclusions overgrow minerals with similar compositions on the vein wall and then become detached.

The vein we have described has a coarse, 'crack–seal' texture. It is coarse in the sense that instead of inclusion bands ours shows host rock fragments and, instead of increments of 10–100 μm wide, ours are typically 0.3–1 mm. The fact that the grain size in the veinlets increases from veinlet walls toward the center demonstrates that open fluid-filled cavities probably existed, into which the veinlet crystals grew. The vein described here, perhaps more than many other published examples, could have been formed by cracking followed or accompanied by sealing.

Li and Means (1997) through some intriguing experiments have shown that fibrous veins, which may otherwise be attributed to the crack–seal mechanism, may be produced without significant fluid flow along vein walls. Their observations are consistent with a model where the vein forms antitaxially by crystallization of the vein material at the wall without the cracking proposed in the 'crack–seal' model. Li and Means (1997) propose, following Taber (1916), that force of crystallization is responsible for vein opening. In this model solute is delivered by diffusion through the porous, fine-grained substrate to the vein. As a consequence, the fibrous nature of some veins may not be caused by crack–seal at the scale of the vein but

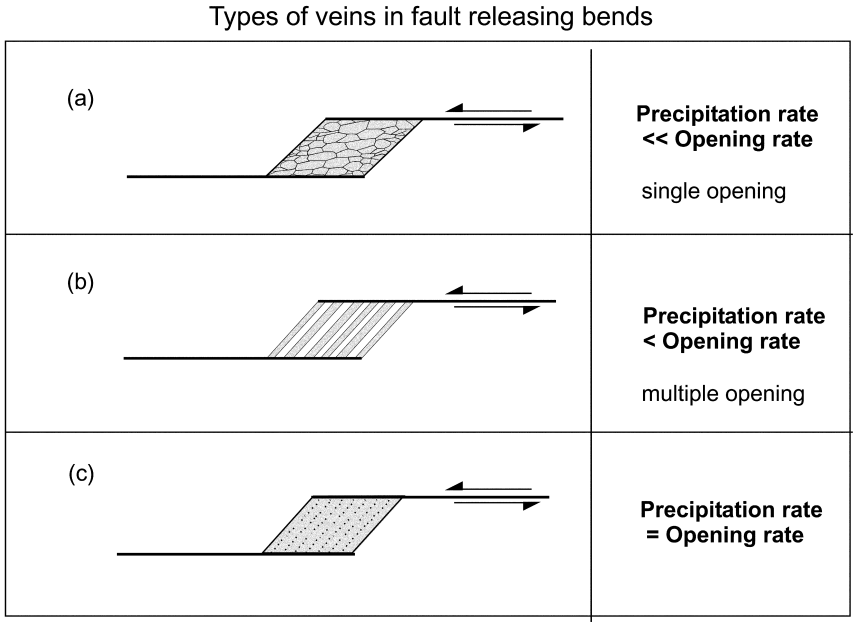

Fig. 12. Types of veins produced from the opening scenarios of Fig. 11. The relative rates of opening and filling give rise to variation in vein fabric. Shaded pattern is calcite and host is unpatterned.

instead is a continuous process of crystal nucleation and growth at the vein–host contact. Wiltschko and Morse (1998; 1999, in review) propose that inclusion trails reflect accidents of crystallization, changes in composition of the fluid, or, in proportion to the amount of trace minerals, simply the composition of the fluid. We propose that the term 'crack–seal', since it implies a process, be restricted to cases where cracking leading to open space can unequivocally be demonstrated.

However, having no preserved open space we must entertain the possibility that none existed as predicted by the force of crystallization models and experiments. The intriguing possibility is that vein formation aided faulting. In this scenario an early-formed normal fault provides a conduit for fluid. Precipitation within left-stepping left-slipping dilational jogs causes displacement parallel to the fault. It is interesting that some isolated faults in the Austin Chalk are reported to decrease in displacement up and down dip, as one would predict if faulting were caused by a proscribed region of precipitation. However, this slip distribution is not unique to this fault growth mechanism.

6. Conclusions

The development of the multi-layered crack–seal vein in this study can be described as calcite precipitation induced by an opening-and-sealing process. (1) More than 3‰ difference in oxygen isotope values between two end-points in the vein also indicates that the vein had developed by a sequential opening process. (2) The veinlets are clearly syntaxial with vein growth most likely into open space, although no evidence of this open space (i.e. vugs) remains. (3) The ratio of host to vein material is nearly 1:1, which explains the difference between the apparent length of the vein and the true fault offset. (4) Veins of this type occur along overlapping left-stepping, left-slipping fault segments, or dilatant jogs, on normal faults. These veins display true crack–seal texture, although the process by which they formed could, over-all, have been nearly continuous; i.e. aseismic fault creep, rather than episodic (microseismic) slip.

Acknowledgements

Support for this research was provided by: (1) Center for Energy and Mineral Resources, Texas A&M University, (2) Interdisciplinary Research Initiative Program, Texas A&M University, and (3) Texas Advanced Research Program (No. 010366-159), the State of Texas to D. V. Wiltschko and (4) Center for Mineral Resources Research, Korea University, to Y.-J. Lee. Discussions with Kevin Corbett and Jin-Han Ree were helpful. Ethan Grossman and Horng-Sheng Mii provided their kind instruction during the oxygen and carbon isotope analyses for the vein sample. Thanks to Allan Walsh, Alamo Cement Co., for graciously granting us access to the Longhorn Quarry. We wish to thank Don Fisher, Stephen Cox and an anonymous reviewer for their helpful reviews.

References

Brown, T.E., Waechter, N.B., Rose, P.R., Barnes, B.E., 1983. Geologic Atlas of Texas: San Antonio Sheet. The University of Texas at Austin, Bureau of Economic Geology, Austin, Texas.

Cloud, K.W., 1975. The diagenesis of the Austin Chalk. M.S. thesis, University of Texas at Dallas, Dallas, Texas.

Collins, E.W., Lauback, S.E., Vendeville, B.C., 1990. Faults and fractures in the Balcones Fault Zone, Austin region, central Texas, Austin Geological Society, Guidebook, 13, pp. 1–24.

Corbett, K.P., Friedman, M., Spang, J., 1987. Fracture development and mechanical stratigraphy of Austin Chalk, Texas. American Association of Petroleum Geologists Bulletin 71, 17–28.

Cox, S.F., 1987. Antitaxial crack–seal vein microstructure and their relationship to displacement paths. Journal of Structural Geology 9, 779–787.

Cox, S.F., Etheridge, M.A., 1983. Crack-seal fibre growth mechanisms and their significance in the development of oriented layer silicate microstructures. Tectonophysics 92, 147–170.

Davison, I., 1995. Fault slip evolution determined from crack-seal veins in pull-aparts and their implications for general slip model. Journal of Structural Geology 17, 1025–1034.

Durney, D.W., Ramsay, J.G., 1973. Incremental strains measured by syntectonic crystal growths. In: DeJong, K.A., Scholten, R. (Eds.), Gravity and Tectonics. John Wiley and Sons, New York, pp. 67–96.

Etheridge, M.A., Wall, V.J., Cox, S.F., Vernon, R.H., 1984. High fluid pressures during regional metamorphism and deformation: implications for mass transport and deformation mechanisms. Journal of Geophysical Research 89, 4344–4358.

Fisher, D.M., Brantley, S.L., 1992. Models of quartz overgrowth and vein formation; deformation and episodic fluid flow in an ancient subduction zone. Journal of Geophysical Research 97, 20043–20061.

Fisher, D.M., Brantley, S.L., Everett, M., Dzvonik, J., 1995. Cyclic flow through a regionally extensive fracture network within the Kodiak accretionary prism. Journal of Geophysical Research 100, 12881–12894.

Friedman, M., 1967. Description of rocks and rock masses with a view toward their mechanical behavior. Proceedings of the first Congress of the International Society of Rock Mechanics III, Lisbon, Portugal, 181-197.

Gaviglio, P., 1986. Crack–seal mechanism in a limestone: a factor of deformation in strike-slip faulting. Tectonophysics 131, 247–255.

Grabowski, G.J., 1984. Generation and migration of hydrocarbons in Upper Cretaceous Austin Chalk, south-central Texas. In: Palacas, J.G. (Ed.), Geochemistry and Source Rock Potential of Carbonate Rocks, American Association of Petroleum Geologists, Studies in Geology, 18, pp. 97–116.

Hulin, C.D., 1929. Structural control of ore deposition. Economic Geology 24, 15–49.

Jackson, M.P.A., 1982. Fault tectonics of the East Texas Basin. The University of Texas at Austin, Bureau of Economic Geology, Geological Circular, 82-4.

Jessell, M.W., Willman, C.E., Gray, D.R., 1994. Bedding parallel veins and their relationship to folding. Journal of Structural Geology 16, 753–767.

Labaume, P., Berty, C., Laurent, Ph., 1991. Syn-diagenetic evolution of shear structures in superficial nappes: an example from the Northern Apennines (NW Italy). Journal of Structural Geology 13, 385–398.

Lee, Y.-J., Wiltschko, D.V., Grossman, E.L., Morse, J.W., Lamb, W.M., 1997. Sequential vein growth with fault displacement in the Austin Chalk Formation, Texas. Journal of Geophysical Research 102, 22611–22628.

Li, T., Means, W.D., 1997. Taber growth of fibrous veins. Geological Society of America Abstracts with Programs 29, A161.

Ohlmacher, G.C., Aydin, A., 1997. Mechanics of vein, fault and solution surface formation in the Appalachian Valley and Ridge, northeastern Tennessee, U.S.A.: implications for fault friction, state of stress and fluid pressure. Journal of Structural Geology 19, 927–944.

Ramsay, J.G., 1980. The crack–seal mechanism of rock deformation. Nature 284, 135–139.

Ramsay, J.G., Huber, M.I., 1987. The Techniques of Modern Structural Geology, Volume 2: Folds and Fractures. Academic Press, London.

Segal, P., Pollard, D.D., 1980. Mechanics of discontinuous faults. Journal of Geophysical Research 85, 4337–4350.

Taber, S., 1916. The growth of crystals under external pressure. American Journal of Science 41, 532–556.

Urai, J.L., Williams, P.F., van Roermund, H.L.M., 1991. Kinematics of crystal growth in syntectonic fibrous veins. Journal of Structural Geology 13, 823–836.

Wiltschko, D.V., Morse, J.W., 1998. Force of crystallization origin for veins: crystallization pressure versus fluid pressure as the driving force for vein opening. Geological Society of America Abstracts with Programs 30, A197.